Advances in characterization of soil clay mineralogy using X-ray diffraction: from decomposition to profile fitting

F. Hubert[a], L. Caner[a], A. Meunier[a] & B. Lanson[b]

[a]*HydrASA, University of Poitiers, INSU-CNRS, 40 Avenue du Recteur Pineau, F-86022 Poitiers Cedex, France, and* [b]*Mineralogy & Environments Group, LGCA, Maison des GéoSciences, Grenoble University, CNRS, F-38041 Grenoble Cedex 9, France*

Summary

Structural characterization of soil clay minerals often remains limited despite their key influence on soil properties. In soils, complex clay parageneses result from the coexistence of clay species with contrasting particle sizes and crystal chemistry and from the profusion of mixed layers with variable compositions. The present study aimed to characterize the mineralogy and crystal chemistry of the <2 µm fraction along a profile typical of soils from Western Europe and North America (Neo Luvisol). X-ray diffraction (XRD) patterns were interpreted using: (i) the combination of XRD pattern decomposition and indirect identification from peak positions commonly applied in soil science; and (ii) the multi-specimen method. This latter approach implies direct XRD profile fitting and has recently led to significant improvements in the structural characterization of clay minerals in diagenetic and hydrothermal environments. In contrast to the usual approach, the multi-specimen method allowed the complete structural characterization of complex clay parageneses encountered in soils together with the quantitative analysis of their mineralogy. Throughout the profile, the clay paragenesis of the studied Neo Luvisol systematically includes discrete smectite, illite and kaolinite in addition to randomly interstratified illite-smectite and chlorite-smectite. Structural characteristics of the different clay minerals, including the composition of mixed layers, did not vary significantly with depth and are thus indicative of the parent material. The relative proportion of the <2 µm fraction increased with increasing depth simultaneously with smectite relative proportion. These results are consistent with the leaching process described for Luvisols in the literature.

Introduction

The <2 µm fraction of soils is commonly dominated by clay minerals that control, to a large extent, important soil chemical and physical properties such as cation exchange capacity and specific surface area (Dixon & Weed, 1989). In addition, clay minerals record the pedogenetic history of soils (see the review of Wilson, 1999). An accurate determination of clay mineralogy and of its changes along the soil profile is thus essential for both purposes. Two main factors impede such a precise identification: first, soil clay parageneses are most often mixtures of clay species with a variety of particle sizes (50 nm to 5 µm), and crystal-chemistry; second, soil clay minerals are often mixed layers with variable compositions (Righi & Elsass, 1996).

Over the last decade, the combined use of DecompXR (Lanson, 1997) and Newmod (Reynolds, 1985) has improved the interpretation of X-ray diffraction (XRD) patterns in soils. DecompXR allows the decomposition of complex diffraction maxima into elementary peaks characterized by their positions, full width at half-maximum intensity (FWHM) and intensities. This approach thus reveals the phase heterogeneity of samples and allows quantifying compositional changes within a series of samples, for example in a soil profile. However, the decomposition by itself does not allow the identification of mixed layers; that is, the determination of the different layer types coexisting within crystallites, their proportion and their stacking sequences. Mixed-layer identification is routinely performed from the comparison of experimental peak positions with those calculated, commonly using Newmod, for mixed layers whose composition (nature and proportion of the different layer types) and stacking parameters are optimized.

Such a combination of XRD pattern decomposition and Newmod calculations has been successfully applied to samples from diagenetic or hydrothermal geological settings (Lanson & Besson, 1992). It has been used for soils to: (i) evaluate the effect of time on soil formation (Righi & Meunier, 1991; Righi *et al.*, 1995; Hardy *et al.*, 1999; Egli *et al.*, 2001, 2008; Velde

Correspondence: F. Hubert. E-mail: fhubert@etu.univ-poitiers.fr

et al., 2003; Vingiani *et al.*, 2004; Montagne *et al.*, 2008); (ii) investigate the role of vegetation cover (Barré *et al.*, 2007a) and of macrofauna (Jouquet *et al.*, 2007) on clay mineralogy; and (iii) characterize the interactions between clay minerals and organic matter in relation to carbon sequestration (Fontaine *et al.*, 2007). However, this dual procedure allows only an approximate characterization of the mixed layers as the identification relies essentially on peak position without fitting the complete reflection profiles including asymmetries and shoulders. Profile fitting results in a more reliable identification of mixed layers (Drits, 2003). Fitting simultaneously the profiles of various basal reflections provides additional constraints.

To overcome the intrinsic limitations of the previous approaches, the profile fitting method calculates a complete XRD pattern from a structural model optimized for each clay species present (Drits & Sakharov, 1976; Drits & Tchoubar, 1990). Drits *et al.* (1997a) and Sakharov *et al.* (1999a,b) further improved the approach as several structural models may fit a given experimental pattern equally well. In the multi-specimen method, the optimized structural model should describe all XRD patterns obtained for a given sample following different treatments, such as saturation by different interlayer cations, ethylene glycol solvation, heating, etc., equally well. The multi-specimen method can be applied to mixed layers with more than two layer types whatever the layer stacking sequences, and there is no *a priori* limitation to the nature of identified species. It provides also quantitative phase analysis of complex clay parageneses (Drits, 2003).

Over the last decade, the multi-specimen method has been widely used to characterize clay mineralogy and its evolution in diagenetic and hydrothermal series (Drits *et al.*, 1997a, 2002a,b, 2004, 2007; Sakharov *et al.*, 1999a,b, 2004; Lindgreen *et al.*, 2000, 2002; Claret *et al.*, 2004; McCarty *et al.*, 2004, 2008; Inoue *et al.*, 2005; Aplin *et al.*, 2006; Lanson *et al.*, 2009). Compared with diagenetic and hydrothermal clay pargeneses, soil clay species are poorly crystallized and numerous randomly interstratified mixed layers could coexist. To our knowledge, this method has never been applied to soil samples before the present study, which investigates the <2 μm fraction mineralogy of a Luvisol typical of Western Europe and North America (Jamagne *et al.*, 1984; Velde, 2001). We aimed to demonstrate that, compared with the common identification approach using decomposition and indirect comparison with calculated patterns, profile fitting provides new insights into soil clay mineralogy, allowing a more reliable and more complete identification of clay species and the quantification of their relative proportions. This is essential for the understanding of soil genesis and dynamics. A second aim was to investigate whether the redistribution of clay species between soil horizons and the limited changes of clay crystal structures were consistent with a leaching process.

Materials and methods

Soil samples

The studied soil is a 'Neo Luvisol' according to the World reference base (IUSS working group WRB, 2006). It is developed on loess deposits from the Closeaux Field Experiment, at the Experimental Station of the Institut National de la Recherche Agronomique (INRA – Château de Versailles, France).

On the basis of field observations, five horizons were sampled from the soil profile. Noticeable marks of hydromorphy were observed in the E1g, E2g, Bt and Bt/C horizons, together with accumulation of clays in the pore system of the Bt/C horizon. The relative proportion of the <2 μm fraction steadily increased with increasing depth from 18% in the surface horizon to 27% in the deeper ones (Table 1). In addition, CEC at the soil pH increased with the increasing content of the <2 μm fraction from 11.2 cmol(c) in Ap to 16.7 cmol(c) in Bt/C. The content of organic carbon decreased from 1.6% in the surface horizon to 0.2% in the Bt/C horizon. Finally, the carbonate content was negligible throughout the soil profile, and the cation exchange complex was predominantly saturated with calcium (Ca) (Moni, 2008).

Separation of the <2 μm fraction for X-ray diffraction analysis

No chemical treatments were applied to the raw samples as routine removal of organic matter by using H_2O_2, or of iron and aluminium oxy-hydroxides by using the dithionite-citrate-bicarbonate protocol (Mehra & Jackson, 1960; Moore & Reynolds, 1997), may alter the clay minerals and more especially mixed-layer species (Velde *et al.*, 2003). Samples from each soil horizon were first

Table 1 Main chemical and physical features of the soil profile studied (adapted from Moni, 2008)

Horizon	Depth / cm	Particle size fraction / μm			OC	CaCO$_3$ eq.	pH	CECe	Exchangeable cations			
		0–2	2–50	50–2000					Ca^{++}	Mg^{++}	Na$^+$	K$^+$
		/ %			/ g kg^{-1}				/ cmol (c)kg^{-1}			
Ap	0–30	18	57	25	16.10	<1	6.5	11.2	9.73	0.90	0.03	0.57
E1g	30–45	19	61	20	6.36	1.8	7.2	12.1	11.50	0.86	0.04	0.18
E2g	45–80	21	50	29	3.95	<1	7.5	12.8	11.27	0.92	0.04	0.18
Bt	80–100	24	47	29	3.38	1.1	7.7	14.6	11.50	1.35	0.05	0.20
Bt/C	100–135	27	48	25	1.80	<1	7.9	16.7	12.03	1.81	0.08	0.27

OC= organic carbon; CaCO$_3$ eq.= calcium carbonate equivalent; CECe= cation exchange capacity at soil pH.

air-dried and sieved to <2 mm; 100 g of the sieved sample was then mixed with deionized water and disaggregated by using agitation with glass balls. The <50 µm fraction was separated next by wet-sieving and dispersed using ultrasonic treatment (20 minutes at 600 W for 400 ml of suspension: Balesdent *et al.*, 1998). The <2 µm fraction was subsequently isolated from the silt (2–50 µm) by using repeated siphoning of the dispersed material (settling for 18 hours at 20°C and removal of the upper 22 cm). The extracted suspension was centrifuged, and the remaining supernatant was filtered to 0.45 µm and added to the centrifugation 'residue', which was then freeze-dried. The clay minerals were studied in their natural state. Consistent with their natural saturation by Ca, a repeated Ca-saturation test (five repeats) did not reveal any difference between natural and Ca-saturated samples (XRD data not shown).

Oriented mounts of the <2 µm fraction were prepared by using the filter transfer method (0.2 µm Nucleopore® polycarbonate filters, Whatman, Maidstone, UK), as recommended by Moore & Reynolds (1997) for quantitative XRD analysis. Aliquots of 50 mg were deposited on a silicon wafer to avoid scattering from glass. XRD patterns were obtained using a Panalytical X'pert Pro diffractometer (PANalytical B.V., Almelo, The Netherlands) equipped with an X'celerator detector ($CuK\alpha_{1+2}$ radiation) in the air-dried state (AD) at room humidity (approximately 35%) and after solvation with liquid ethylene glycol (EG). The sizes of the divergence, two Soller and antiscatter slits were 0.5, 2.3, 2.3 and 0.5°, respectively. Diffraction data were recorded in a scanning mode and converted to step patterns (with a step of $0.017°2\theta$ from 2.5 to $35°2\theta$, using a 200-second counting time per step).

Decomposition of XRD patterns

Decomposition of AD and EG patterns was performed as recommended by Lanson (1997) over the $3–14°2\theta$ range. Over this angular range, the resolution of the $K\alpha_{1+2}$ doublet is low enough to allow using the Fityk 0.8.2 peak fitting software (Wojdyr, 2007). Following background stripping, XRD patterns were fitted with Gaussian elementary curves whose number was steadily increased until a satisfactory fit to the data was obtained. The initial parameters (position and FWHM) of elementary curves were derived from previous studies on similar soil clay parageneses (Righi *et al.*, 1995; Pernes-Debuyser *et al.*, 2003) and optimized with the Levenburg-Marquardt algorithm. When compared, the results obtained were identical to those of DecompXR (data not shown).

X-ray profile modelling method

XRD patterns of the five samples were modelled, in both AD and EG states, with the Sybilla© software developed by Chevron™ (Aplin *et al.*, 2006). This program provides a graphic user interface to the algorithm developed initially by Drits & Sakharov (1976) and used recently by Drits *et al.* (1997a) and Sakharov *et al.* (1999a,b). It allows the direct comparison between experimental and calculated XRD profiles, the latter being the sum of all elementary contributions that have been identified.

Instrumental and experimental parameters such as horizontal and vertical beam divergence, goniometer radius and slide length were introduced and not further refined. The sigmastar parameter (σ^*), which characterizes the distribution of particle orientation, was set for each clay mineral phase as recommended by Rüping *et al.* (2005). For all layer types z atomic coordinates proposed by Moore & Reynolds (1997) were used after modification to fit the layer thickness values used for simulation; thermal motion parameters (B) were also set as proposed by Moore & Reynolds (1997). The position and amount of interlayer species (H_2O and EG molecules in particular) were considered as variable parameters and varied about the values proposed by Moore & Reynolds (1997) during the fitting process. In bi-hydrated smectite layers (2w) a single plane of H_2O molecules was assumed to be present on each side of the interlayer mid-plane as proposed by Ferrage *et al.* (2005a,b). Illite and smectite structural formulae were similar to those proposed by Laird *et al.* (1991) from the ICP-AES elemental analysis of the <2 µm fraction from similar soils (Table 2).

For each mixed layer, the number, nature, proportion and stacking sequences of the different layer types were considered as adjustable parameters. In the AD state and under room humidity conditions, expandable layers may be dehydrated (S0w: $d_{001} \simeq$ 1.00 nm), mono-hydrated (S1w: $d_{001} \simeq$ 1.25 nm), or bi-hydrated states (S2w: $d_{001} \simeq$ 1.50 nm) (Ferrage *et al.*, 2005b). Illite and S0w layers cannot be differentiated in the AD state, but smectite layers expand following EG solvation to incorporate one or two sheets of EG molecules in their interlayers (S1eg: $d_{001} \simeq$ 1.30 nm, and S2eg: $d_{001} \simeq$ 1.68 nm, respectively; Table 2). Finally, the distributions of coherent scattering domain sizes (CSDSs) were assumed to be lognormal and characterized by their mean value (Drits *et al.*, 1997b). The quality of the fit was estimated with the unweighted R parameter (Howard & Preston, 1989) over

Table 2 Structural characteristics of the different clay layers

Layer type	Layer thickness / nm	Interlayer cation content[a]	Octahedral iron content[a]
Discrete illite	1.000	1.5	0.0
Illite in mixed layers	1.000	1.0	0.5
Smectite (S1w)[b]	1.250	0.5	1.2
Smectite (S2w)[b]	1.500	0.5	1.2
Smectite (S1eg)[b]	1.300	0.5	1.2
Smectite (S2eg)[b]	1.680	0.5	1.2
Chlorite	1.420	–	0.0
Kaolinite	0.716	–	–

[a]Number of atoms per formula unit.
[b]S1w= smectite with one sheet of interlayer H_2O molecules; S2w = smectite with two sheets of interlayer H_2O molecules; S1eg = smectite with one sheet of interlayer EG molecules; S2eg = smectite with two sheets of interlayer EG molecules.

the 4–35°2θ and the 3.5–35°2θ ranges for AD and EG patterns, respectively, to minimize the influence of the low-angle region where the effect of X-ray scattering becomes significant. The 19–22°2θ and 26.5–27.0°2θ ranges were excluded for the calculation of R as they contain peaks other than clay 00*l* reflections. For practical reasons, optimization was performed using a trial-and-error approach without automatic refinement of the parameters. To ensure the reliability of the model, both AD and EG patterns of a given sample were fitted with a unique set of structural parameters. The relative proportions of the different clay species in these complex parageneses were also optimized with Sybilla. The multi-specimen approach requires that these proportions be similar in both AD and EG states.

Results

Qualitative description of experimental XRD patterns

XRD patterns obtained on the <2 μm fraction (AD and EG) of the five soil horizons are shown in Figure 1. All samples contained quartz (0.426 and 0.334 nm peaks), feldspars (0.325 and 0.320 nm) and poorly crystallized goethite (0.418 nm). The clay paragenesis is similar for all horizons including kaolinite (rational series of peaks at 0.716 and 0.358 nm in AD and EG states) and illite-mica (rational series of peaks at 1.01, 0.498 and 0.334 nm in AD and EG states). In addition, the presence of broad and irrational peak series whose position shifts between AD and EG treatments suggests the presence of mixed layers containing expandable layers. Specifically, the 1.47 nm peak observed on the AD pattern shifted to approximately 1.75 nm following EG solvation. Such behaviour is characteristic of randomly interstratified illite-smectite (Moore & Reynolds, 1997). The steady intensity increase of the 1.47 nm peak with increasing depth suggests an

increasing proportion of this mixed layer from Ap to Bt horizons. Finally, the presence of a maximum peaking at 0.485 nm, and its behaviour following EG solvation, supports the presence of a mixed layer containing both chlorite and expandable layers.

XRD pattern decomposition results

The number of elementary contributions (six and seven in AD and EG states, respectively) necessary to fit the data was remarkably similar for all samples, as are their positions, FWHMs, and relative intensities (Figure 2). This overall similarity supports the hypothesis of a constant composition for all clay minerals along the soil profile. The illite-mica peak at approximately 1.00 nm was fitted by using a broad band at 1.020 nm and a sharp one at 1.000 nm, most probably accounting for a broad CSDS distribution. Similarly, the kaolinite peak at 0.716 nm was fitted with broad and sharp maxima peaking at 0.730 and 0.716 nm, respectively. The broad contribution at approximately 1.47 nm was fitted, also using two elementary contributions. The broad contribution at 1.500 nm (1.550 nm for the Bt/C horizon) sharpens, shifts to 1.750 nm and presents an additional peak at 0.930 nm after EG solvation. The sharp peak at 1.460 nm (AD) broadened and shifted to 1.580 nm after EG solvation.

In their study of a similar soil, Pernes-Debuyser *et al.* (2003) used NEWMOD to identify the clay minerals present in surface samples. These authors attributed the two bands at 1.450 nm (broad) and 1.540 nm (sharp) to two randomly interstratified illite-smectite having similar contents of illite and S2w layers (50:50) but different CSDS distributions (one to four and three to six layers, respectively). The XRD pattern corresponding to this clay paragenesis was calculated using Sybilla and compared with the data (Figure 3) to assess the validity of the identification proposed by Pernes-Debuyser *et al.* (2003). The profiles of the peaks
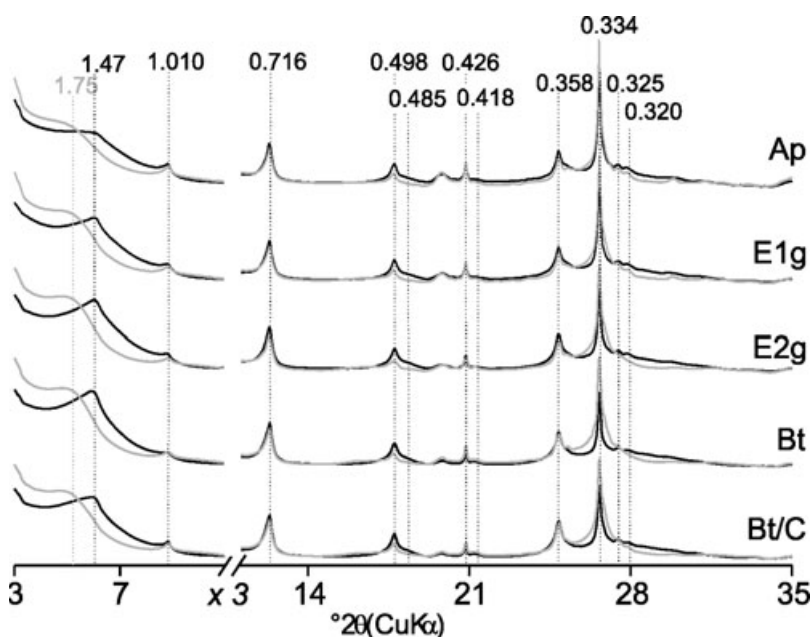

Figure 1 Experimental XRD patterns obtained for the <2 μm fraction of the five soil horizons. Black and grey solid lines represent XRD patterns recorded in AD and EG states, respectively. Dashed lines indicate the positions of the main reflections (peak positions in nm).
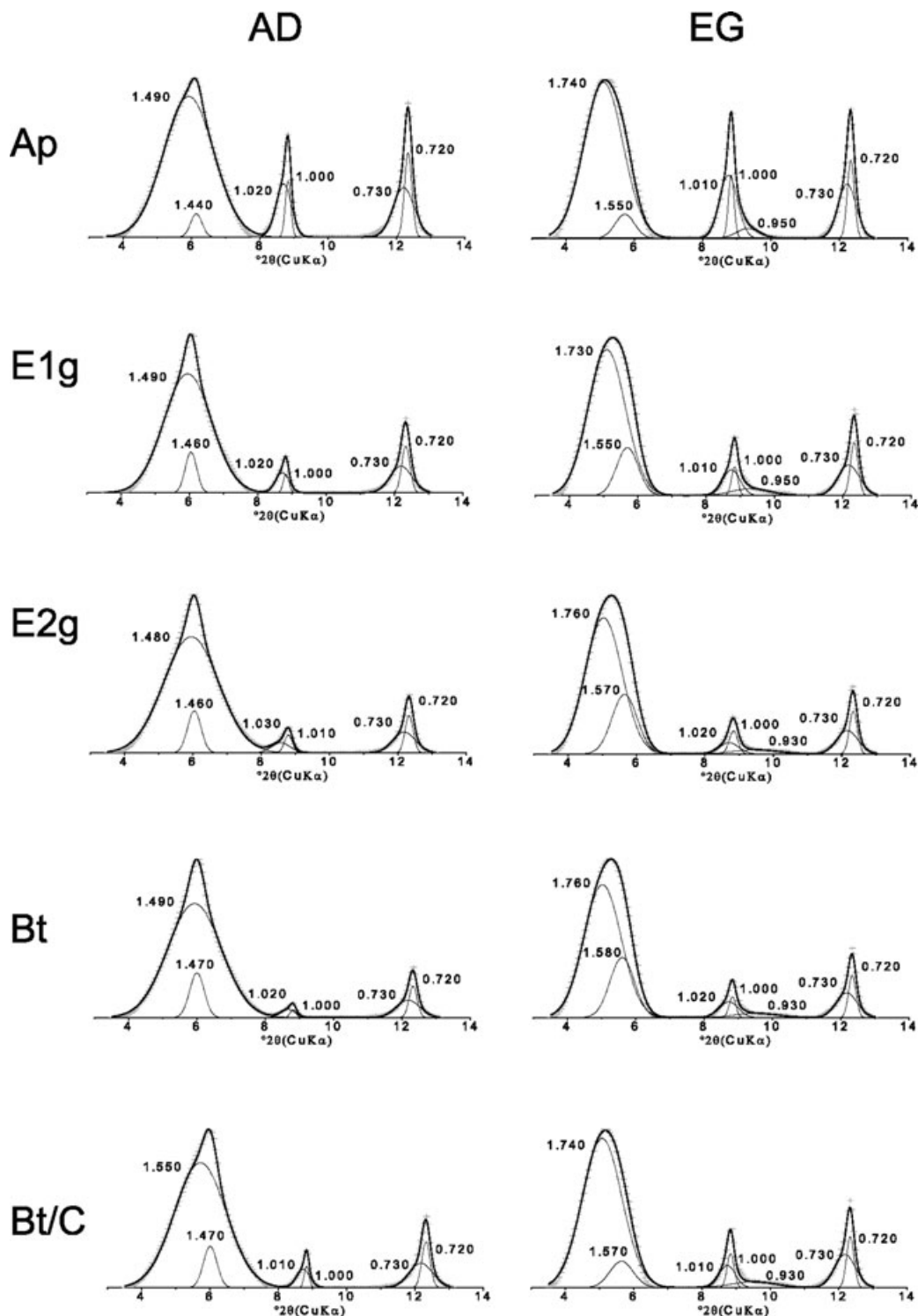
Figure 2 Decomposition of XRD data. The experimental XRD patterns and the best fit are shown as grey crosses and as solid lines, respectively. Elementary Gaussian contributions are shown as solid grey lines.
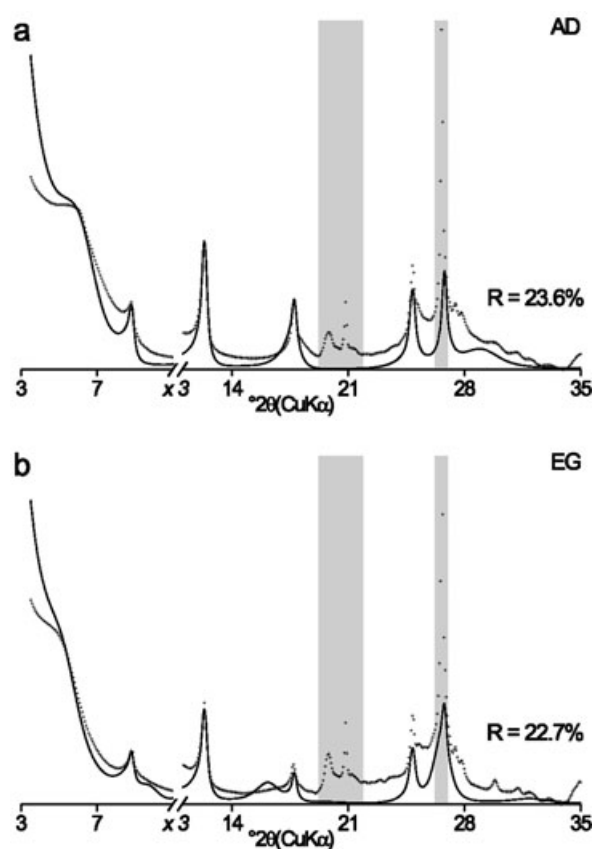
Figure 3 Comparison between experimental (grey crosses) and calculated (solid lines) XRD patterns for the Ap horizon. (a) AD pattern; (b) EG pattern. The calculated pattern corresponds to the clay paragenesis determined by Pernes-Debuyser *et al.* (2003) for a similar Ap horizon. The broken x-axis indicates a modified scale factor (× 3) for the high-angle region. The grey boxes correspond to angular ranges excluded for the calculation of the quality-of-fit estimate (R parameter).

corresponding to discrete kaolinite and illite were satisfactorily reproduced. The overall profile of the low-angle data, especially that of the EG patterns, was also approximately reproduced. Significant mismatches were, however, observed, especially over the 6–11, 14–19 and 26–35°2θ ranges, that resulted in an overall poor fit (Figure 3; R = 23.6% and 22.7% for AD and EG states, respectively) and therefore refute the identification proposed by Pernes-Debuyser *et al.* (2003). In particular, the chlorite-expandable mixed layer whose presence was hypothesized from the maximum peaking over the 18–19°2θ range at 0.485 nm (AD) has a probable contribution over the low-angle region.

Full pattern fitting

To overcome the limitations of an indirect identification illustrated above, XRD patterns recorded on the oriented clay separates preparations of all horizons were all fitted in both AD and EG states. The optimum fit was obtained systematically with randomly interstratified illite–smectite and chlorite–smectite, in addition

to discrete smectite, illite and kaolinite as illustrated for the Bt horizon (Figure 4). The structural characteristics of the optimal models are listed in Tables 2 and 3, and Table 4 contains the relative proportions of the different contributions. Discrete illite contributed to the three reflections at 1.006, 0.499 and 0.333 nm (AD) and 1.001, 0.501 and 0.333 nm (EG). These reflections were sharp, indicative of a large mean CSDS (18 layers – Table 3). Two populations of kaolinite having contrasting CSDS (6–20 layers on average) were necessary to fit the low-angle asymmetry of the 0.716 and 0.358 nm reflections. At 1.554 nm, the 001 reflection of discrete smectite contributed significantly to the overall intensity of the broad 1.47 nm peak. The 005 reflection (0.305 nm) also accounted for the high-angle tail of the peak at 0.334 nm (AD). Following EG solvation, the first smectite reflection shifted to 1.808 nm, accounting for the low-angle asymmetry of the peak at 1.750 nm. The 005 reflection at 0.337 nm contributed to the large 'background' intensity between the 0.358 and 0.334 nm peaks. Discrete smectite has a small mean CSDS (three layers) to match the width of experimental maxima. The heterogeneous hydration and swelling behaviours (36:64 S1w:S2w ratio in the AD state, and 24:76 S1eg:S2eg ratio after EG salvation; Table 3) also contribute to line broadening. The 003 reflection of smectite has a low intensity compared with that of 001 because of the large content of octahedral iron (1.2 atoms by unit formula; Table 2, Laird *et al.*, 1991).

A randomly interstratified illite-smectite with a large illite content (63:37 illite:smectite ratio) was also identified in the clay paragenesis. This mixed layer has a small CSDS (six layers) and its smectite layers exhibited a heterogeneous hydration and swelling behaviour (Table 3). As a result, its first order reflection (at approximately 1.27 nm in the AD state) allowed the high-angle asymmetry of the 1.47 nm peak to be fitted, whereas the 0.503 and 0.322 nm maxima contributed to the low- and high-angle tails of the complex maxima at 0.498 and 0.334 nm, respectively (Figure 4a). Following EG solvation, this randomly interstratified illite-smectite exhibited only weak and poorly-defined modulations over the low-angle region, which makes it essentially undetectable using a decomposition approach. This mixed layer thus contributed to the diffracted intensity mostly on the high-angle side of the 0.498 nm peak, and in the complex band at 0.334 nm. A randomly interstratified chlorite-smectite (52:48 chlorite:smectite ratio; Table 3) completed the clay paragenesis accounting in particular for the high angle shoulder of the 0.498 nm peak (AD) and for the sharp maximum of the broad 1.47 nm band (Figure 4a). After EG solvation, this mixed layer contributed mostly to the large 'background' intensity between the 0.358 and 0.334 nm peaks, and to the complex 1.75 nm band.

The same clay paragenesis with discrete kaolinite, illite and smectite, and randomly interstratified illite–smectite and chlorite–smectite, was used to fit XRD patterns from all five horizons (Figure 5, Tables 3 and 4) with R factor values ranging from 8.7 to 12.8% and from 9.3 to 12.6% for AD and EG patterns, respectively. The structural characteristics of discrete illite and kaolinite were essentially constant over the entire soil
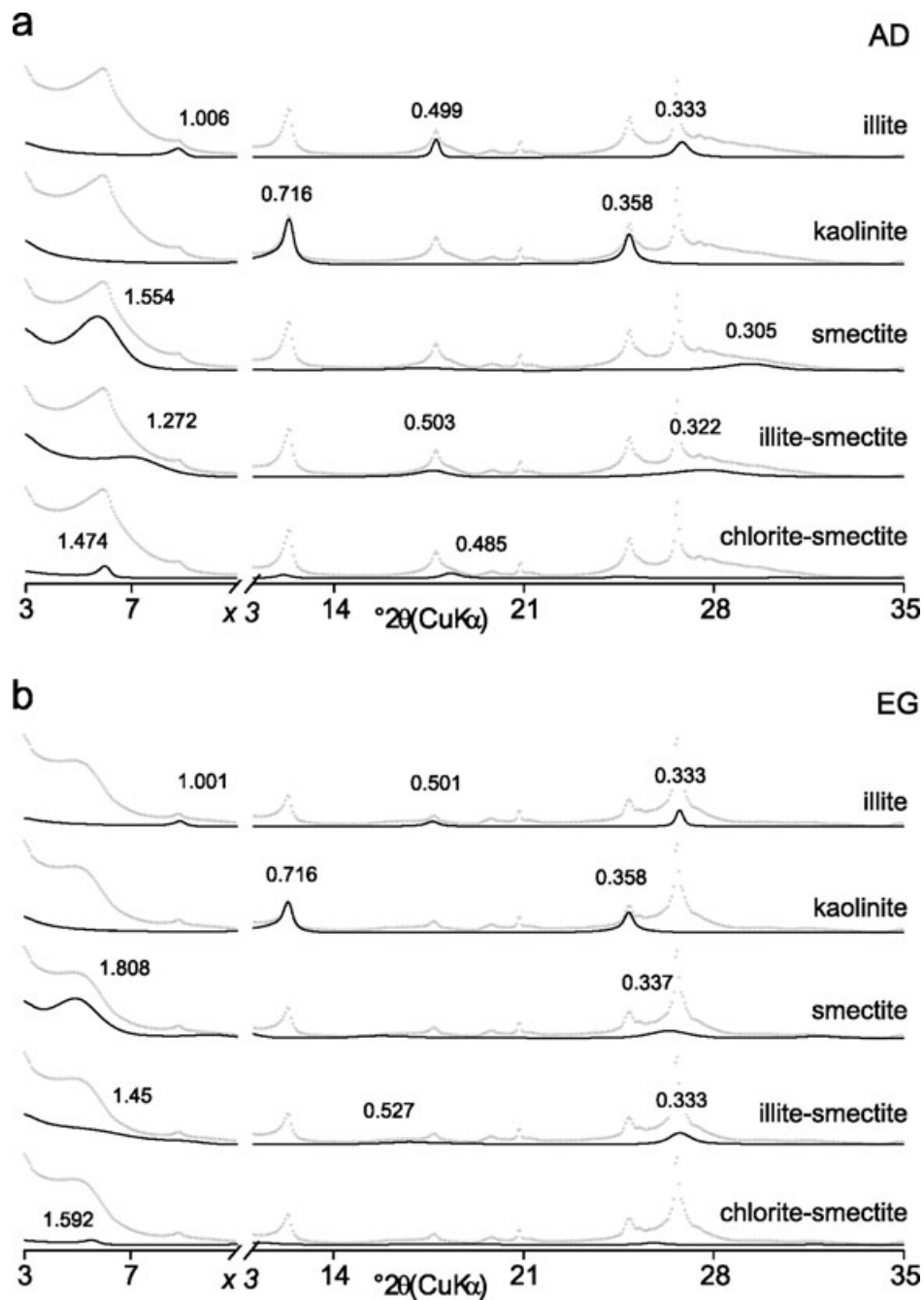
Figure 4 Elementary contributions to the diffracted intensity for the Bt horizon. Patterns as for Figure 3. The broken *x*-axis indicates a modified scale factor (× 3.0) for the high-angle region. (a) AD pattern; (b) EG pattern. The positions of the main maxima are given in nm. The kaolinite contribution includes the two sub-populations having different CSDS. The structural parameters for the optimal models are given in Tables 2 and 3, the relative proportions of the different contributions in Table 4.

profile. Similarly, discrete smectite was systematically dominated by S2w layers (AD), the relative proportion of which was at a minimum in E1g and E2g horizons at approximately 55%, and increased to 77% in the Bt/C horizon. Following EG solvation, most smectite layers incorporated two sheets of EG molecules. Consistent with the hydration behaviour, the proportion of S2eg

layers was minimal in the E1g horizon (72%) and maximal in Bt/C (94%).

The composition of the two mixed layers was also more or less constant along the soil profile, with 63% illite in the illite–smectite and 52% chlorite in the chlorite–smectite, except in the most superficial horizon (62% chlorite). In both mixed layers, the

Table 3 Composition and structural characteristics (in per cent weight) of clay minerals in the different soil horizons

Phases	Horizon	Ap	E1g	E2g	Bt	Bt/C
Illite	$\sigma*$	17	17	17	17	17
	CSDS	18	18	18	18	18
	I/S2w[a]	98/2	97/3	97/3	95/5	97/3
	I/S2eg[a]	98/2	97/3	97/3	97/3	97/3
Kaolinite	σ *	18	18	18	18	18
	CSDS	20	20	20	20	20
Kaolinite	σ *	18	18	18	18	18
	CSDS	6	6	6	6	6
Smectite	σ *	21	21	21	21	21
	CSDS	3	3	3	3	3
	S1w/S2w[a]	33/67	46/54	47/53	36/64	23/77
	S1eg/S2eg[a]	21/79	28/72	17/83	24/76	6/94
Illite-smectite (R0)	σ *	17	17	17	17	17
	CSDS	9	6	6	6	7
	I/S1w/S2w[a]	63/6/31	63/13/24	63/11/26	63/13/24	63/7/30
	I/S1eg/S2eg[a]	57/13/30	63/7/30	63/3/34	63/8/29	63/3/34
Chlorite-smectite (R0)	σ *	17	17	17	17	17
	CSDS	7	9	9	9	9
	Ch/S1w/S2w[a]	62/13/25	52/11/37	52/6/42	52/2/46	52/8/40
	Ch/S1eg/S2eg[a]	62/0/38	52/0/48	52/6/42	52/0/48	52/0/48

[a]S1w = smectite with one sheet of interlayer H_2O molecules; S2w = smectite with two sheets of interlayer H_2O molecules; S1eg = smectite with one sheet of interlayer EG molecules; S2eg= smectite with two sheets of interlayer EG molecules; I = illite layers both in discrete illite and in mixed layers.
σ* = parameter characterizing the orientation of particles on the X-ray slide.
CSDS = coherent scattering domain size expressed in layers.

Table 4 Relative proportions (in per cent weight) of the different contributions to the diffracted intensity

Sample		Illite	Kaolinite (large CSDS)	Kaolinite (small CSDS)	Smectite	Illite-smectite	Chlorite-smectite
Ap	AD	20	12	9	18	33	8
	EG	18	9	10	18	38	7
E1g	AD	22	11	9	24	28	6
	EG	21	9	9	27	29	5
E2g	AD	18	11	9	25	31	6
	EG	17	11	8	26	33	5
Bt	AD	18	11	7	33	24	6
	EG	17	10	7	32	26	8
Bt/C	AD	21	12	8	23	30	6
	EG	18	11	9	23	32	7

CSDS = coherent scattering domain size; AD = results obtained on the air-dried preparation; EG = results obtained after ethylene glycol solvation.

hydration behaviour of expandable layers was heterogeneous, with 4–35% of smectite layers having only one sheet of interlayer H_2O molecules. Following EG solvation, swelling heterogeneity was reduced, especially in the chlorite–smectite (Table 3). In the illite–smectite, swelling heterogeneity was more pronounced, with 8–30% of smectite layers incorporating a single sheet of EG molecules, the proportion of S1eg steadily decreasing with increasing depth.

Relative proportions of the various clay species are listed in Table 4. Discrete illite and kaolinite represent approximately 20% of the <2 μm fraction each, their proportion being constant throughout the profile. The proportion of discrete smectite increased from the Ap (18%) to the Bt horizon (33%) in which it was the dominant clay species. At greater depth in the Bt/C horizon, the proportion of discrete smectite decreased to 23%. The randomly interstratified illite-smectite was the dominant clay species throughout the soil profile, except in the Bt horizon, despite its diffuse contribution to the low-angle intensity (Figure 4b). From E2g to Bt horizons, the proportion of this mixed layer decreased from approximately 30 to approximately 25%, increasing again to approximately 30% in the Bt/C horizon. Finally, the chlorite-smectite accounts for 5–8% of the <2 μm fraction along the soil profile, without any significant change with depth.

Discussion

In the present work, pattern fitting led to an innovative interpretation of XRD patterns, providing detailed information on the different phases present in the soil horizons, on their structural evolution and on their relative abundances. In the following discussion the fitting approach will first be compared with numerical tools commonly used for the interpretation XRD patterns (DecompXR, Newmod). The results in terms of pedogenesis will then be discussed.
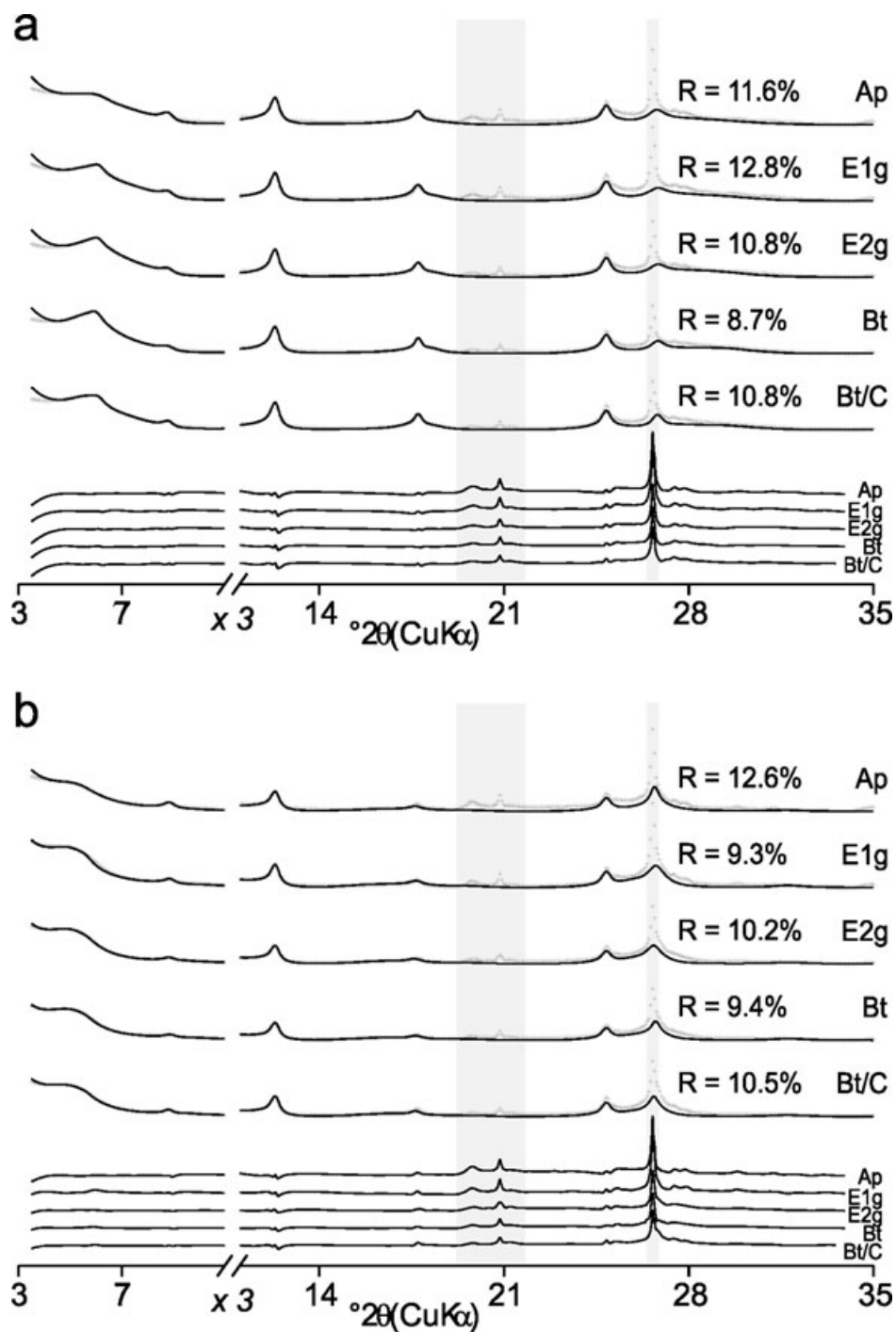
Figure 5 Comparison between experimental XRD patterns (grey crosses) and optimum multi-specimen fits (solid line) for the five horizons (Ap, E1g, E2g, Bt and Bt/C) of the Luvisol. (a) Air-dried and (b) EG solvated samples. Difference plots are shown at the bottom of the Figure. The structural parameters used for these fits are provided in Tables 2 and 3, the relative proportions of the different contributions in Table 4.

Limitations of the decomposition-XRD calculation approach

The present study allows us to question the combined use of XRD pattern decomposition and indirect identification from elementary peak positions (± FWHM) to describe complex clay parageneses commonly encountered in soils, although it has been widely used for this purpose over the last decade (Righi *et al.*, 1995; Righi & Elsass, 1996; Velde, 2001; Pernes-Debuyser *et al.*, 2003; Velde *et al.*, 2003; Vingiani *et al.*, 2004; Jouquet *et al.*, 2005, 2007; Fontaine *et al.*, 2007; Barré *et al.*, 2007a,b, 2008a,b; Montagne

et al., 2008). In particular, the clay mineralogy deduced from such a data processing (illite, kaolinite and two randomly interstratified illite–smectite, Pernes-Debuyser *et al.*, 2003), did not permit the reproduction of XRD data for the samples investigated. Several hypotheses can be proposed to account for this inadequacy.

The first is the specific diffraction fingerprint, without any significant peak in the low-angle region, of the randomly interstratified illite–smectite, which is the main clay mineral phase in the soil profile. This mixed layer is characterized by a broad and poorly defined contribution to the diffracted intensity. As a consequence, this major contribution is stripped during the initial background removal. This key drawback of the decomposition approach is especially noteworthy for soil clay minerals, as most of them combine small CSDS and complex interstratification, thus giving rise to weakly modulated XRD patterns.

The second hypothesis, that indirect identification of mixed layers from their peak position is essentially inadequate, is discussed in detail by Lanson (2005). Specifically, the heterogeneous nature of expandable interlayers hampers the use of simplified peak migration identification techniques based on two-component mixed layers (Drits, 1997, 2003). Such hydration/swelling heterogeneity has been found in most natural samples, whatever their origin and mineralogy (Drits *et al.*, 1997a; Sakharov *et al.*, 1999a; Lindgreen *et al.*, 2000; Drits, 2003; McCarty *et al.*, 2004; Inoue *et al.*, 2005; Ferrage *et al.*, 2005b, 2007). Again, this drawback is especially important for soils where heterogeneity is expected to be even greater than in other geological settings.

New contributions from XRD profile-fitting for interpreting complex clay mineral assemblages

The overall agreement, both visually (Figure 5) and quantitatively with R values systematically being <13%, demonstrates the ability of the multi-specimen approach to provide a good quality fit to experimental data obtained on polyphasic soil samples: this is consistent with previous studies in other geological settings (Drits *et al.*, 1997a, 2002a,b, 2004, 2007; Sakharov *et al.*, 1999a,b, 2004; Lindgreen *et al.*, 2000, 2002; Claret *et al.*, 2004; McCarty *et al.*, 2004, 2008; Inoue *et al.*, 2005; Aplin *et al.*, 2006; Lanson *et al.*, 2009). This approach can thus be used to determine accurate structural characteristics for the phases present in a given sample, as well as their relative proportions. The sensitivity of the approach to structural characteristics and phase heterogeneity has been discussed previously (Drits *et al.*, 1997a, 2002b, 2007; Sakharov *et al.*, 1999a; Drits, 2003; Lanson *et al.*, 2009). However, the actual sensitivity of the calculated XRD patterns to key structural characteristics needs to be illustrated. The actual presence of the different contributions is the first of these. In the present work, mixed layers are introduced only if they allowed fitting specific angular ranges without significant overlap with other phases as illustrated in Figure 4. The absence of the small CSDS kaolinite contribution leads, for example, to a significant misfit over the 11–12°2θ range (Figure 6a). The influence of CSDS is illustrated next. Compared with the optimal
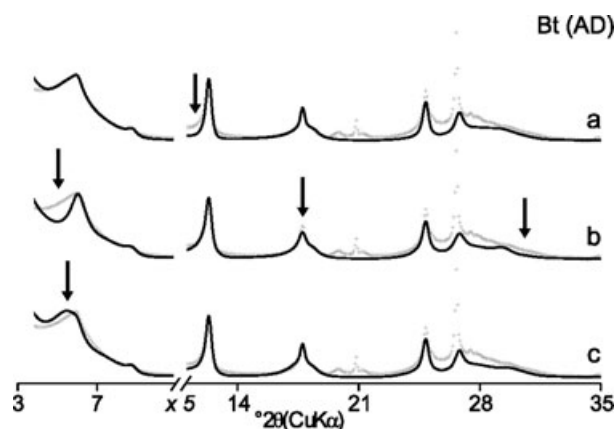

Figure 6 Sensitivity of calculated XRD patterns to the mineralogical composition and structural characteristics. Arrows indicate significant misfits compared with the optimum fit shown in Figure 5(a) (Bt horizon). The optimum structural characteristics and mineralogical composition are given in Tables 3 and 4, respectively. (a) XRD pattern calculated without the contribution of kaolinite having low CSDS. (b) CSDS of discrete smectite are increased from three (optimum) to five layers whereas those of discrete illite are decreased from 17 (optimum) to 13 layers. (c) All layers are considered to be bi-hydrated in discrete smectite.

fit to the data (Figure 5), increasing the CSDS of discrete smectite from three to five layers leads to evident misfits over the 4–6°2θ and 29.5–31.5°2θ ranges, whereas decreasing the CSDS of discrete illite from 18 to 13 layers decreased the resolution of the peak at 17.5°2θ (002 reflection: Figure 6b). Finally, sensitivity of calculated profiles to smectite hydration behaviour may be assessed by considering, for example, that all layers are bi-hydrated in discrete smectite. As a result, the 001 reflection was shifted towards smaller angles, thus inducing a major misfit over the 4–6°2θ range (Figure 6c).

The next section focuses on the implications of the original description of clay paragenesis obtained from profile fitting for clay pedogenetic processes and more especially for three major issues.

Clay paragenesis in Luvisols. From XRD results, Jamagne *et al.* (1984) claimed that the clay mineralogy is similar in the different horizons of soils formed on loess deposits, even in the case of intense clay illuviation, and indicate that the <2 μm fraction includes kaolinite, mica and a complex group of other layer silicates, including smectite and mixed layers of chloritic, micaceous, vermiculitic and smectitic layers in random interstratification'. Using XRD profile fitting, the present study confirms the interpretation of Jamagne *et al.* (1984) for discrete clay species with the presence of kaolinite, illite and smectite. It also allows an improved description of the 'complex group of other silicates' that includes two randomly interstratified illite–smectite (63:37) and chlorite–smectite (52:48). Direct profile fitting thus confirms that in Luvisols the clay paragenesis is stable along the soil profile as proposed by Jamagne *et al.* (1984).

Structural characteristics of clay species and their development along the profile. Even when looking at a more detailed level, clay mineralogy was remarkably constant along the soil profile. Structural parameters of discrete kaolinite and illite and of illite–smectite and chlorite–smectite phases were similar in the different horizons (Table 3). Some differences were, however, observed at the soil surface. In particular, the chlorite content of the chlorite–smectite increased from 52 to 62% in the topsoil Ap horizon, simultaneously with a decrease of its mean CSDS from nine to seven layers. On the contrary, the mean CSDS of the illite–smectite increases from six to seven layers in the lower horizons to nine layers in the uppermost one (Table 3). The parent material, the loess deposit, was thus probably homogeneous. In addition, kaolinite, illite, illite–smectite and chlorite–smectite species did not present significant structural changes along the soil profile compared with discrete smectite. The hydration and swelling (S1w:S2w and S1eg:S2eg ratios, respectively) properties of smectite varied from one horizon to the other, however, without any significant trend with depth. In addition, the relative proportions of S1w and S1eg layers were not strictly correlated, the latter being usually smaller than the former. Except in the Bt/C horizon where smectite was almost fully expanded after EG solvation, the proportion of S1eg layers ranged from 17 to 28% (Table 4). Consistent with our observations, Velde (2001) reported that approximately one-third of expandable layers incorporated a single sheet of EG molecules in the surface horizons of cultivated soils, and thus deduced the presence of a similar proportion of high-charge expandable layers. However, in our case the heterogeneous swelling observed for discrete smectite is possibly induced by sample preparation artefacts. No sample pre-treatments were performed to remove organic matter and iron oxy-hydroxides prior to size fractionation. Such pre-treatments were performed on sample aliquots to extract the <0.05 μm size fraction. These fractions, which concentrate discrete smectite, were X-rayed following solvation by EG vapour (16 hours at 40°C under vacuum). The results obtained (not shown) showed no difference between Ap and Bt horizons with 100% of S2eg layers in both cases. The intimate mixing of organic matter and/or of iron oxy-hydroxides with clays is thus likely to be responsible for the observed reduced expandability of smectite, and for the observed variation of smectite swelling behaviour along the profile.

Quantitative phase analysis. The direct profile fitting method overcomes the intrinsic limitations of the decomposition approach, which was restricted to peak intensity ratios between similar clay species, and provides reliable estimates of the phase composition for complex clay parageneses (Drits *et al.*, 1997a; Lindgreen *et al.*, 2002; Claret *et al.*, 2004; McCarty *et al.*, 2008; Lanson *et al.*, 2009). Jamagne *et al.* (1984) concluded that the relative contents of mica and trioctahedral chlorite increase close to the soil surface as the result of the physical breakdown of coarse particles and/or of the preferential migration of other minerals as reported also in Belgian soils (Van Ranst *et al.*, 1982). In our work, we show that

the relative proportion of discrete smectite increases from 18% (Ap horizon) to approximately 25% (E1g and E2g horizons) and 33% (Bt horizon, Table 4). This proportion decreases to 25% in the Bt/C horizon. The contribution of discrete smectite increases essentially at the expense of illite–smectite, which dominated the clay paragenesis in all horizons but Bt. Discrete kaolinite and illite and chlorite–smectite were also affected but to a lesser extent because of their smaller abundances. In addition, the increase in the <2 μm fraction content with increasing depth may further attenuate the impact on these clay species. The present results are thus consistent with the leaching process described for Luvisols, and more especially with undisturbed column leaching experiments performed with the same soil (Rousseau *et al.*, 2004).

Conclusions

The present study demonstrates that the combined use of XRD pattern decomposition and indirect identification from peak positions does not allow a complete identification of complex clay parageneses such as those commonly encountered in soils. However, when carefully used (see recommendations of Lanson, 1997), this approach can be a relevant preliminary step in the study of clay mineral evolution in soils formed on homogenous parent materials.

A complete, accurate and quantitative mineralogical characterization of complex clay parageneses requires fitting the data with a pattern calculated for a hypothesized mineral assemblage. Additional constraints can be obtained for a given sample by fitting various XRD patterns obtained after different treatments. Using this multi-specimen approach, structural characteristics and relative proportions of both discrete and mixed layer clays are obtained. The present study demonstrates that, although time-consuming, the multi-specimen approach can be applied to soil samples. The resulting mineralogical characterization of clays can then serve as the basis for studying their individual structural evolution, and that of their relative abundances along the profile.

In particular, it is shown in the present Luvisol profile that the structural characteristics of all clay minerals are essentially constant over the entire profile, thus reflecting the mineralogy of the parent material. As reported in the literature (Duchaufour & Lelong, 1967; Jamagne, 1973; Pedro *et al.*, 1978; Jamagne *et al.*, 1984), pedogenesis ongoing in Luvisols affects, essentially, the vertical distribution of the different clay species as the result of particle migration. Our results indicate that the relative increase of smectite has a major contribution to the overall increase of the <2 μm fraction with increasing depth. This interpretation of the mineralogical data is in agreement with the leaching process described for Luvisols in the literature and may be valid for other soils formed on loess deposits that are common in North America and Western Europe and used to grow crops. As the proposed approach allows us to gain detailed information on the structural evolution of individual clay species, further research could aim at determining the impact of fertilizers, human

activities or plant nutrient uptake on the development of soil minerals. In addition, the complete and quantitative mineralogical characterization allows the comparison of clay parageneses in soils derived from different parent materials.

Acknowledgements

References

Aplin, A.C., Matenaar, I.F., McCarty, D.K. & van der Pluijm, B.A. 2006. Influence of mechanical compaction and clay mineral diagenesis on the microfabric and pore-scale properties of deep-water Gulf of Mexico mudstones. *Clays & Clay Minerals*, **54**, 500–514.

Balesdent, J., Besnard, E., Arrouays, D. & Chenu, C. 1998. The dynamics of carbon in particle-size fractions of soil in a forest-cultivation sequence. *Plant & Soil*, **201**, 49–57.

Barré, P., Velde, B. & Abbadie, L. 2007a. Dynamic role of "illite-like" clay minerals in temperate soils: facts and hypotheses. *Biogeochemistry*, **82**, 77–88.

Barré, P., Velde, B., Catel, N. & Abbadie, L. 2007b. Soil-plant potassium transfer: impact of plant activity on clay minerals as seen from X-ray diffraction. *Plant & Soil*, **292**, 137–146.

Barré, P., Montagnier, C., Chenu, C., Abbadie, L. & Velde, B. 2008a. Clay minerals as a soil potassium reservoir: observation and quantification through X-ray diffraction. *Plant & Soil*, **302**, 213–220.

Barré, P., Velde, B., Fontaine, C., Catel, N. & Abbadie, L. 2008b. Which 2:1 clay minerals are involved in the soil potassium reservoir? Insights from potassium addition or removal experiments on three temperate grassland soil clay assemblages. *Geoderma*, **146**, 216–223.

Claret, F., Sakharov, B.A., Drits, V.A., Velde, B., Meunier, A., Griffault, L. *et al.* 2004. Clay minerals in the Meuse-Heute Marne underground laboratory (France): possible influence of organic matter on clay mineral evolution. *Clays & Clay Minerals*, **52**, 515–532.

Dixon, J.B. & Weed, S.B. 1989. *Minerals in Soil Environments*. Soil Science Society of America Inc., Madison, WI.

Drits, V.A. 1997. Mixed-layer minerals. In: *EMU Notes in Mineralogy*, Volume 1 (ed. S. Merlino), pp. 153–190. Eötvös University Press, Budapest.

Drits, V.A. 2003. Structural and chemical heterogeneity of layer silicates and clay minerals. *Clay Minerals*, **38**, 403–432.

Drits, V.A. & Sakharov, B.A. 1976. *X-ray Structural Analysis of Mixed-layer Minerals*. Nauka, Moscow (in Russian).

Drits, V.A. & Tchoubar, C. 1990. *X-ray Diffraction by Disordered Lamellar Structures: Theory and Applications to Microdivided Silicates and Carbons*. Springer-Verlag, Berlin.

Drits, V.A., Lindgreen, H., Sakharov, B.A. & Salyn, A.L. 1997a. Sequential structure transformation of illite-smectite-vermiculite during diagenesis of Upper Jurassic shales, North Sea. *Clay Minerals*, **33**, 351–371.

Drits, V.A., Srodon, J. & Eberl, D.D. 1997b. XRD measurement of mean crystallite thickness of illite and illite/smectite: reappraisal of the kubler index and the scherrer equation. *Clays & Clay Minerals*, **45**, 461–475.

Drits, V.A., Lindgreen, H., Sakharov, B.A., Jakobsen, H.J., Salyn, A.L. & Dainyak, L.G. 2002a. Tobelitization of smectite during oil generation in oil-source shales. Application to North Sea illite-tobelite-smectite-vermiculite. *Clays & Clay Minerals*, **50**, 82–98.

Drits, V.A., Sakharov, B.A., Dainyak, L.G., Salyn, A.L. & Lindgreen, H. 2002b. Structural and chemical heterogeneity of illite-smectites from Upper Jurassic mudstones of East Greenland related to volcanic and weathered parent rocks. *The American Mineralogist*, **87**, 1590–1607.

Drits, V.A., Lindgreen, H., Sakharov, B.A., Jacobsen, H.J. & Zviagina, B.B. 2004. The detailed structure and origin of clay minerals at the Cretaceous/Tertiary boundary, Stevns Klint (Denmark). *Clay Minerals*, **39**, 367–390.

Drits, V.A., Lindgreen, H., Sakharov, B.A., Jakobsen, H.J., Fallick, A.E., Salyn, A.L. *et al.* 2007. Formation and transformation of mixed-layer minerals by Tertiary intrusives in Cretaceous mudstones, West Greenland. *Clays & Clay Minerals*, **55**, 260–283.

Duchaufour, P. & Lelong, F. 1967. Entraînement et destruction d'argile dans les horizons éluviaux des sols lessivés. *Comptes Rendus de l'Académie des Sciences série D*, **264**, 2884–2887.

Egli, M., Mirabella, A. & Fitze, P. 2001. Clay mineral formation in soils of two different chronosequences in the Swiss Alps. *Geoderma*, **104**, 145–175.

Egli, M., Nater, M., Mirabella, A., Raimondi, S., Plötze, M. & Alioth, L. 2008. Clay minerals, oxyhydroxide formation, element leaching and humus development in volcanic soils. *Geoderma*, **143**, 101–114.

Ferrage, E., Lanson, B., Malikova, N., Plançon, A., Sakharov, B.A. & Drits, V.A. 2005a. New insights on the distribution of interlayer water in bi-hydrated smectite from X-ray diffraction profile modeling of 00l reflections. *Chemistry of Materials*, **17**, 3499–3512.

Ferrage, E., Lanson, B., Sakharov, B.A. & Drits, V.A. 2005b. Investigation of smectite hydration properties by modeling of X-ray diffraction profiles. Part 1. Montmorillonite hydration properties. *The American Mineralogist*, **90**, 1358–1374.

Ferrage, E., Lanson, B., Sakharov, B.A., Geoffroy, N., Jacquot, E. & Drits, V.A. 2007. Investigation of dioctahedral smectite hydration properties by modeling of X-ray diffraction profiles: influence of layer charge and charge location. *The American Mineralogist*, **92**, 1731–1743.

Fontaine, S., Barot, S., Barré, P., Bdioui, N., Mary, B. & Rumpel, C. 2007. Stability of organic carbon in deep soil layers controlled by fresh carbon supply. *Nature*, **450**, 277–280.

Hardy, M., Jamagne, M., Elsass, F., Robert, M. & Chesneau, D. 1999. Mineralogical development of the silt fractions of a Podzoluvisol on loess in the Paris Basin (France). *European Journal of Soil Science*, **50**, 443–456.

Howard, S.A. & Preston, K.D. 1989. Profile fitting of powder diffraction patterns. In: *Modern Powder Diffraction* (eds D.L. Bish & J.E. Post), pp. 217–275. Mineralogical Society of America, Chantilly, VA.

Inoue, A., Lanson, B., Marques-Fernandes, M., Sakharov, B.A., Murakami, T., Meunier, A. & Beaufort, D. 2005. Illite-smectite mixed-layer minerals in the hydrothermal alteration of volcanic rocks: I. One-dimensional XRD structure analysis and characterization of component layers. *Clays & Clay Minerals*, **53**, 423–439.

IUSS working group WRB 2006. *World Reference Base for Soil Resources*. World Soil Resources Reports No. 103. FAO, Rome.

Jamagne, M. 1973. *Contribution à l'étude pédogénétique des formations loessiques du Nord de la France*. PhD thesis, Faculté des Sciences Agronomiques, Gembloux.

Jamagne, M., De Coninck, F., Robert, M. & Maucorps, J. 1984. Mineralogy of clay fractions of some soils on loess in northern France. *Geoderma*, **33**, 319–342.

Jouquet, P., Barré, P., Lepage, M. & Velde, B. 2005. Impact of subterranean fungus-growing termites (Isoptera, Macrotermitiane) on chosen soil properties in a West African savanna. *Biology & Fertility of Soils*, **41**, 365–370.

Jouquet, P., Bottinelli, N., Lata, J.C., Mora, P. & Caquineau, S. 2007. Role of the fungus-growing termite *Pseudacanthotermes spiniger* (Isoptera, Macrotermitinae) in the dynamic of clay and soil organic matter content. An experimental analysis. *Geoderma*, **139**, 127–133.

Laird, D.A., Barak, P., Nater, E.A. & Dowdy, R.H. 1991. Chemistry of smectitic and illitic phases in interstratified soil smectite. *Soil Science Society of America Journal*, **55**, 1499–1504.

Lanson, B. 1997. Decomposition of experimental X-ray diffraction profile (profile fitting): a convenient way to study clay minerals. *Clays & Clay Minerals*, **45**, 132–146.

Lanson, B. 2005. Crystal structure of mixed-layer minerals and their X-ray identification: new insights from X-ray diffraction profile modeling. *Clay Science*, **12** (Suppl. 1), 1–5.

Lanson, B. & Besson, G. 1992. Characterisation of the end of smectite-to-illite transformation: decomposition of x-ray patterns. *Clays & Clay Minerals*, **40**, 40–52.

Lanson, B., Sakharov, B.A., Claret, F. & Drits, V.A. 2009. Diagenetic smectite-to-illite transition in clay-rich sediments: a reappraisal of X-ray diffraction results using the multi-specimen method. *American Journal of Science*, **309**, 476–516.

Lindgreen, H., Drits, V.A., Sakharov, B.A., Salyn, A.L., Wrang, P. & Dainyak, L.G. 2000. Illite-smectite structural changes during metamorphism in black Cambrian Alum shales from the Baltic area. *The American Mineralogist*, **85**, 1223–1238.

Lindgreen, H., Drits, V.A., Sakharov, B.A., Jakobsen, H.J., Salyn, A.L., Dainyak, L.G. *et al.* 2002. The structure and diagenetic transformation of illite-smectite and chlorite-smectite from North Sea Cretaceous-Tertiary chalk. *Clay Minerals*, **37**, 429–450.

McCarty, D.K., Drits, V.A., Sakharov, B., Zviagina, B.B., Ruffell, A. & Wach, G. 2004. Heterogeneous mixed-layer clays from the Cretaceous, Greensand, Isle of Wight, southern England. *Clays & Clay Minerals*, **52**, 552–575.

McCarty, D.K., Sakharov, B.A. & Drits, V.A. 2008. Early clay diagenesis in gulf coast sediments: new insights from XRD profile modeling. *Clays & Clay Minerals*, **56**, 359–379.

Mehra, O.P. & Jackson, M.L. 1960. Iron oxide removal from soils and clay by dithionite-citrate system buffered with sodium bicarbonate. *Clays & Clay Minerals*, **7**, 317–327.

Moni, C. 2008. *Stabilisation physique et physico-chimique de la matière organique dans les horizons profonds du sol*. PhD thesis, Université Pierre et Marie Curie, Paris, p. 6.

Montagne, D., Cornu, S., Le Forestier, L., Hardy, M., Josière, O., Caner, L. *et al.* 2008. Impact of drainage on soil-forming mechanisms in a French Albeluvisol: input of mineralogical data in mass-balance modelling. *Geoderma*, **145**, 426–438.

Moore, D.M. & Reynolds, R.C. Jr 1997. *X-Ray Diffraction and the Identification and Analysis of Clay Minerals*. Oxford University Press, Oxford.

Pedro, G., Jamagne, M. & Begon, J.C. 1978. Two routes in genesis of strongly differentiated acid soils under humid, cool-temperate conditions. *Geoderma*, **20**, 173–189.

Pernes-Debuyser, A., Pernes, M., Velde, B. & Tessier, D. 2003. Soil mineralogy evolution in the INRA 42 plots experiment (Versailles, France). *Clays & Clay Minerals*, **51**, 577–584.

Reynolds, R.C. Jr 1985. *NEWMOD: A Computer Program for the Calculation of One-dimentional Patterns of Mixed-layered Clays*. Reynolds, R.C., Jr, Hanover.

Righi, D. & Elsass, F. 1996. Characterization of soil clay minerals: decomposition of X-ray diffraction diagrams and high-resolution electron microscopy. *Clays & Clay Minerals*, **44**, 791–800.

Righi, D. & Meunier, A. 1991. Characterization and genetic interpretation of clays in an acid brown soil (Dystrochrept) developed in a granitic saprolite. *Clays & Clay Minerals*, **39**, 519–530.

Righi, D., Velde, B. & Meunier, A. 1995. Clay stability in clay-dominated soil systems. *Clay Minerals*, **30**, 45–54.

Rousseau, M., Di Pietro, L., Angulo-Jaramillo, R., Tessier, D. & Cabibel, B. 2004. Preferential transport of soil colloidal particles: physicochemical effects on particle mobilization. *Vadose Zone Journal*, **3**, 247–261.

Rüping, K., Dohrmann, R., Jahn, R. & Kleber, M. 2005. Texturmessungen an Tonmineralen in orientierten Präparaten - Eine kritische Diskussion zur Tonmineralquantifizierung. In: *DTTG 2005* (eds R. Dohrmann & S. Kaufhold), pp. 56–72. Deutsche Ton-und Tonmineralgruppe e.V., Celle.

Sakharov, B.A., Lindgreen, H., Salyn, A.L. & Drits, V.A. 1999a. Determination of illite-smectite structures using multispecimen XRD profile fitting. *Clays & Clay Minerals*, **47**, 555–566.

Sakharov, B.A., Lindgreen, H. & Drits, V.A. 1999b. Mixed-layer kaolinite-illite-vermiculite in North Sea shales. *Clay Minerals*, **34**, 333–344.

Sakharov, B.A., Dubinska, E., Bylina, P., Kozubowski, J.A., Kapro, G. & Frontczak-Baniewicz, M. 2004. Serpentine-smectite interstratified minerals from Lower Silesia (SW Poland). *Clays & Clay Minerals*, **52**, 55–65.

Van Ranst, E., De Coninck, F., Tavernier, R. & Langohr, R. 1982. Mineralogy in silty to loamy soils of central and high Belgium in respect to autochthonous and allochthonous materials. *Bulletin de la Société Belge de Géologie*, **91**, 27–44.

Velde, B. 2001. Clay minerals in the agricultural surface soils in the Central United States. *Clay Minerals*, **36**, 277–294.

Velde, B., Goffé, B. & Hoellard, A. 2003. Evolution of clay minerals in a chronosequence of poldered sediments under the influence of a natural pasture development. *Clays & Clay Minerals*, **51**, 205–217.

Vingiani, S., Righi, D., Petit, S. & Terribile, F. 2004. Mixed-layer kaolinite-smectite minerals in a red-black soil sequence from basalt in Sardinia (Italy). *Clays & Clay Minerals*, **52**, 473–483.

Wilson, M.J. 1999. The origin and formation of clay minerals in soils: past, present and future perspectives. *Clay Minerals*, **34**, 7–25.

Wojdyr, M. 2007. *Fityk 0.8.2 Free Software*. Wojdyr, M.[WWW document]. URL http://www.unipress.waw.pl/fityk [accessed on 12 May 2009]. Warsaw.